Title

Inferring Ancient Technology and Practices of the Elite Maya Kingship Through the Application of Materials Engineering Characterization Modalities

Author

Cheung, Kristina

Publication Date

2014

Peer reviewed|Thesis/dissertation

UNIVERSITY OF CALIFORNIA

Los Angeles

Inferring Ancient Technology and Practices of the Elite Maya Kingship Through the Application of Materials Engineering Characterization Modalities

A thesis submitted in partial satisfaction

of the requirements for the degree of Master of Science

in Materials Science and Engineering

by

Kristina Alyssa Cheung

2014

ABSTRACT OF THE THESIS

Inferring Ancient Technology and Practices of the Elite Maya Kingship Through the Application of Materials Engineering Characterization Modalities

by

Kristina Alyssa Cheung

Master of Science in Materials Science and Engineering

University of California, Los Angeles, 2014

Professor Ioanna Kakoulli, Chair

This project focuses on the characterization of materials from burial offerings and painted decoration in a royal Maya tomb at El Zotz, Guatemala, and their association with mortuary rituals. Archaeological findings included vessels, jade masks, organic materials (wood, cord, and textiles), specular hematite cubes, shells with powdered cinnabar, green (malachite) painted stucco assumed to have decorated the wooden bier where the king was resting, and caches of lip-to-lip Aguila Orange bowls containing human phalanges. This paper describes findings from non-invasive and non-destructive analytical techniques including XRF, VPSEM-EDS, and XRD, emphasizing the potential of these combined technologies in the identification of organic and inorganic markers to infer burial customs. The nature and location of the findings, the evidence of pigment coloration on the bones employing hematite and cinnabar, and the indication of exposure of the bones to high temperatures suggest highly complex, even protracted mortuary practices of Maya elite.

The thesis of Kristina Alyssa Cheung is approved.

Kanji Ono

Christian Fischer

Ioanna Kakoulli, Committee Chair

University of California, Los Angeles

2014

DEDICATION

I would like to dedicate this thesis to my Lord and Savior, Jesus Christ. He has blessed me with the opportunity to pursue research and is the source of any success I have. May everything I accomplish in life be for His glory.

I also dedicate this to my family and friends for their continual love and support throughout my academic endeavors. Special thanks to my parents, Adolf and Marilou Cheung, for never letting me give up.

TABLE OF CONTENTS

LIST OF FIGURES

ACKNOWLEDGEMENTS

The research conducted for this study was supported by the UCLA Graduate Division, Graduate Opportunity Fellowship and the Faculty Research Grant, Academic Senate.

The materials, methodology, preliminary results, and discussion of this research were based on co-authored work published on October 15, 2013 in *Archaeological Chemistry VIII: ACS Symposium Series,* Vol. 1147, Chapter 21, pp 397-418 (Chapter DOI: 10.1021/bk-2013-1147.ch021). Co-authors Stephen Houston, Sarah Newman, Edwin René Román-Ramírez, and Thomas Garrison contributed the archaeological samples and information regarding their context and the excavation. Co-authors Nuoya Xie, Zhaoying Yao, Christian Fischer, Vanessa Muros, and Sergey Prikhodko assisted with sample analysis and interpretation. Ioanna Kakoulli was the principal investigator of this publication.

I would also like to thank Magdalena Balonis-Sant, Xiao Ma, and the UCLA Archaeomaterials Group for their steadfast support throughout this work.

Finally, I would like to express the deepest appreciation to my committee chair and adviser, Dr. Ioanna Kakoulli, who mentored me since my undergraduate years at UCLA and has been a constant source of encouragement, inspiration, and guidance. Her confidence in my work and desire to see me succeed has helped me to grow both academically and personally.

1 Introduction

Archaeological materials science holds much promise for understanding and interpreting ancient civilizations and technology by studying the material culture. This has drawn a large, rapidly growing research effort, much of which has been directed mainly towards the study of ancient manufactured materials (both organic and inorganic) such as ceramic, glass, metals, textiles and basketry, as well as the study of human remains. Despite the potential of the application of modern science modalities in archaeology, the heterogeneous, fragile, and often invaluable nature of archaeological materials poses several limitations in their analysis and interpretation. The methodology and analytics for the characterization of these samples is therefore pivotal for this type of study.

The objective of this research is to identify and employ enabling technologies by applying materials engineering principles and advanced characterization methods to pressing challenges in the study of important archaeological materials. In this arena, this project employs innovative, minimally invasive, non-destructive tools for the characterization of burial offerings and other funerary paraphernalia from an important Maya royal burial ground in Guatemala, which dates between A. D. 350 and A. D. 400. Objects in the tomb that were sampled include wooden and bone artifacts, textiles, painted stucco, and cord. This research presents data to inform the chemistry and properties of these materials and their greater significance to ancient craftsmanship, social organization, and funerary practices of the Maya elite.

One critical aspect is that the archaeological materials recovered from the Maya royal tomb at El Zotz were partially altered both physically and chemically. To better resolve between alteration and original materials, the analysis of these artifacts was based on a multiscale and multianalytical approach from the macro to the molecular length scale, using stereo microscopy (SM), digital microscopy (DM), field emission gun (FEG) variable pressure scanning electron

microscopy (VPSEM) coupled with energy dispersive x-ray spectroscopy (EDS); Raman microspectroscopy (μRS), X-ray fluorescence (XRF) spectroscopy, ultraviolet/visible/near infrared reflectance (UV/Vis/NIR) spectroscopy, and micro X-ray diffraction (XRD). The combination of these techniques provided not only complementary analytical information but also enabled the use of the same sample for multiple analyses with minimal sample preparation and handling.

1.1 Archaeological Context

The royal tomb of an ancient Maya king was discovered below the El Diablo pyramid at El Zotz, one of many Maya archaeological sites in northern Guatemala. The site is located in the San Miguel La Palotada Biotope in the Municipio of San José in the Department El Petén, in the center of the Maya Biosphere Reserve. El Zotz contains over 230 buildings with several pyramidal shaped structures *(1)*. Among these, on a natural elevation, lies the El Diablo, seemingly built for defensive purposes in Early Classic period (AD 250-550). This complex retains parts of decorated architectural façades, a palace, funerary temples, as well as residential areas *(2)*.

Preliminary exploration of El Zotz began in the 1970s, but was excavated more systematically starting in 2006 as part of the El Zotz Archaeological Project, funded by the National Endowment for the Humanities (NEH) and the National Science Foundation (NSF). The excavation was motivated by several reasons: 1) its location, with Tikal to the east and El Peru to the west; 2) the connection to the royal family of Yaxchilan in the Usumacinta River; 3) its geopolitical role in the central area of El Petén during the Maya Classic period (AD 250-900), and 4) how the Maya adopted and modified the physical landscape from the Preclassic (1000 BC- AD 250) to the Postclassic (AD 900-early sixteenth century) period *(2-4)*.

In 2009, excavations along the base of one of the pyramids, structure F8-1 (Figure 1), at the El Diablo complex uncovered elaborate stucco decoration (Figures 2 and 3). In the following season (2010), the archaeological team, led by Stephen Houston from Brown University, discovered an undisturbed tomb (Burial 9), measuring 3.12 m long, 1.25 m wide and 1.50 m high (Figure 4). The well-preserved tomb contained the remains of an adult male, along with six child sacrifices *(3,5)*. This main burial is believed to belong to the first king of El Zotz, possibly Chak' "Fish-Dog" Ahk *(2)* venerated by descendants for at least 100 years with funerary ceremonies reflecting how Maya elites perceived their world. The body most likely held an obsidian blade, which may have been used for human sacrifice, as indicated by the signs of bone-cutting on the blade and the discovery of vessels housing the remains of six children, four of them infants, two others a few years older.

Archaeological findings in Burial 9 included vessels and jade masks, shells, and organic materials (wood, cord, and textiles). Also found were 15 specular hematite ingots, shells with powdered cinnabar, and green painted stucco assumed to have decorated the wooden bier where the king was resting (Figure 6). In addition, caches of lip-to-lip Aguila Orange bowls were found, some of which contained human remains such as extracted teeth and severed digits (Figure 7) *(2,5)*. These objects inside the tomb, along with the surrounding ornate stucco masks representing the ancient Sun God of the Maya society, point to the affluence of this royal figure. In addition, the nature and position of the findings, the evidence of pigment coloration on the bones employing hematite and cinnabar, and the indication of exposure of the bones to high temperatures suggest elaborate and complex mortuary practices of the Maya elite at El Zotz.

2 Materials and Methods

2.1 Archaeological samples

Fourteen archaeological samples (Figures 8 to 18) were analyzed in this study, including organic specimens resembling wood, basket, cord, bone, pseudomorphic textiles, clay, hematite pigment from large cubes found in the tomb (Figure 6), fragments of green painted stucco, red pigment powders found inside shells, and white powder that was covering some human bones in a lip-to-lip cache vessel found outside the tomb. The short outline given for the samples in the captions below (in bold) is based on the description given by the archaeologists during excavation/sampling.

2.2 Sample preparation

Minute quantities of material, in powder or bulk form, were removed from representative areas of the fragmentary archaeological specimens and prepared for analysis using two main types of samples: dispersions and polished cross-sections. Unmounted samples and sample powders were also used accordingly.

2.2.1 Dispersion samples

For the preparation of dispersion samples, a few particles from each specimen were removed by scraping from the areas of interest and placed on a clean glass microscope slide. Meltmount™ thermoplastic resin with RI=1.62, was melted using a double boiler on a hot plate (50° C) and dropped over the particles. A glass cover slip was positioned on the top of the glass microscope slide and then put on a hot plate to allow the resin to become soft. Using an eraser tip from a standard pencil, mild pressure was exerted over the glass cover slip dispersing the particles in the resin while removing all trapped air. This provided a semi-permanent mount for the particles to be analyzed under transmitted polarized light.

2.2.2 Polished cross-sections

For the preparation of cross-sections, stratigraphic or bulk samples (~2 mm^3) were removed from each archaeological specimen using the point of a scalpel. Owing to the small size and multilayered structure of the samples, a special preparation technique was used for embedding *(6)*. Buehler EpoxiCure® epoxy resin (mixed with EpoxiCure® Epoxy Hardener as prescribed) was poured into custom-made rubber cubic molds (1.5x1x1cm) to fill half of their volume. After hardening of the resin, the sample itself was then placed in the mold with the outer surface (top surface) facing downwards. More resin was then poured over the sample until it was completely covered and put under vacuum using a Buehler Cast n' Vac 1000. Once the resin had set, the samples were cut perpendicular to the outer surface using Buehler silicon carbide grinding papers from 240 to 600 grit. Due to the water-sensitive nature of most of the samples, grinding and polishing could not be done with water-based emulsions. Samples were ground using ethanol and dry polished using Micro-Mesh® polishing pads from 1500 to 8000 grit until a well-polished surface was established. In some cases wet polishing was carried out using the alcohol-based Leco® Ultra Lap Diamond Extender Part No. 812-433 together with Leco® Microid Diamond Compounds Part No. 810-871of 3 microns and Part No. 810-870 of 1 micron. Polishing suspensions were spread on Buehler® MasterTex polishing cloths attached to the Leco® GP-25 polishing turntable.

2.3 Characterization methods

The specimens in Table I were analyzed qualitatively and quantitatively using different characterization techniques to infer information on their chemistry, microstructure, and properties. All samples displayed some degree of physical and chemical alteration due to the burial environment, and therefore detailed and systematic analysis was necessary. To distinguish between products of alteration and original materials, the analysis of the samples

involved the application of combined characterization techniques spanning multiple scales, such as stereomicroscopy (SM); digital microscopy (DM); polarized light microscopy (PLM); X-ray fluorescence (XRF) spectroscopy; X-ray diffraction (XRD); ultraviolet/visible/near infrared reflectance (UV/Vis/NIR) spectroscopy; field emission gun (FEG) scanning electron microscopy (SEM) at variable pressure (VP) coupled with energy dispersive X-ray spectroscopy (EDS); and Raman spectromicroscopy (μRS). The combination of these non-invasive and non-destructive imaging and analytical techniques provided complimentary information and enabled the use of the same sample for multiple analyses with minimal sample preparation and manipulation.

2.3.1 Stereomicroscopy (SM), Digital Microscopy (DM) and Polarized Light Microscopy (PLM)

Initial observations of the unmounted samples were recorded using an Omano stereomicroscope between 7x and 45x magnification and a Canon PowerShot A630 digital camera. These samples were also examined under a KEYENCE VHX-1000 digital microscope at 20x, 50x, 100x, and 200x magnification, focusing on specific areas of interest in each sample, which would be later analyzed using VPSEM-EDS.

Dispersion samples of pigmented areas were analyzed using a Leica DMRM polarized light microscope under plane polarized and cross polarized light. The habit, color, pleochroism, relief, refractive index, birefringence, and extinction angles were used to characterize each particle phase identified in the sample.

2.3.2 X-Ray Fluorescence (XRF) spectroscopy

For elemental analysis, the Thermo Scientific Niton® XL3t Series GOLDD™ technology portable XRF was used (pXRF), with a silver anode and silicon drift detector. Readings were taken with an 8mm diameter spot size in both Soil Mode and Mining Mode for 120 seconds for

each measurement. In situ study of the samples with this technique gave qualitative and semi-quantitative information regarding the relative concentrations of major, minor, and trace elements found in each sample and complemented other microanalyses.

2.3.3 X-Ray Diffraction (XRD)

XRD analysis was performed on the pigment powder samples and on Sample 09, which contained the green painted layer on white stucco. For the analysis, a few particles of the area of interest were mounted on a glass spindle and analyzed using a Rigaku R-Axis Spider X-ray diffractometer. XRD spectra were recorded at 50 kV/40 mA using a Cu-Kα target for 900 seconds. XRD data was processed and matched against reference spectra from the International Center for Diffraction Data (ICDD) files using the JADE, v8.2 software from Materials Data Inc.

2.3.4 Ultraviolet/Visible light/Near Infrared (UV/Vis/NIR) reflectance spectroscopy

UV/Vis/NIR spectroscopy was performed using the FieldSpec3® 3 by Analytical Spectral Devices Inc (ASD), with high spectral resolution (3 nm @ 700 nm and 10 nm @ 1400/ 2100 nm) and wide spectral range between 350-2500 nm. The flexible spot size analyzer for contact analysis facilitated the systematic study of specific areas. The high spectral and spatial resolution of the spectrometer was particularly useful for fingerprint identification of different mineral phases and organic compounds in the samples due to its high sensitivity to both the electron transitions in the visible part of the spectrum and the overtones from the organic molecules in the near infrared.

2.3.5 Scanning Electron Microscopy (SEM) and Energy Dispersive X-Ray Spectroscopy (EDS)

Analysis was performed using an FEI Nova™ NanoSEM 230 scanning electron microscope (SEM) with field emission gun and variable pressure capabilities, equipped with a Thermo Scientific NORAN System 7 X-ray Energy Dispersive Spectrometer (EDS).

All archaeological specimens were first examined non-invasively at low vacuum without the need for a conductive coating sputtered over the surface risking to damage, dehydrate, and alter the delicate nature of the specimens. Images providing topographical details of the samples were obtained using a secondary electron (SE) detector using a Low Vacuum Detector (LVD). For this analysis, each sample was placed on an aluminum foil holder, which was secured to the SEM stub using double-sided carbon tape. In addition, samples were blown with compressed air before being placed inside the SEM chamber to remove any loose surface debris. Chamber pressure for all in situ analyses was held at 50 Pa.

Polished cross-sections were also analyzed with SEM-EDS for spatially resolved inter- and intra-layer visualization and elemental characterization. A Gaseous Analytical Detector (GAD) in variable pressure was used for the detection of backscattered electrons (BSE), providing images with compositional contrast; atoms of heavier elements elastically scatter electrons more strongly compared to those of lighter elements, resulting in higher signal intensity for elements with higher atomic numbers. Thus, areas of the sample that are mostly composed of heavy elements appear brighter than areas composed of light elements in an image obtained using BSE, providing useful information when studying the heterogeneous and multi-layered samples.

Elemental spectra and maps of characteristic x-ray photon emissions were acquired using EDS. The analysis of well-polished surfaces was crucial for more precise quantitative

measurements because of the shallow probing depth of electrons interacting with the surface. In addition, flat surfaces minimize the deflection of BSE in different directions, maximizing the collection of electrons by the detector located symmetrically about the incident beam of electrons. EDS spot analysis enabled comparisons of peak intensities, providing data regarding relative concentration of elements found in the specimen, and elemental mapping of certain areas provided a visual of the profile distribution of certain elements.

2.3.6 Raman Spectromicroscopy (μRS)

Analysis using Raman spectromicroscopy (μRS) was conducted with a Renishaw inVia system, using a red laser of wavelength 750 nm. Spectra were first obtained in extended mode before static mode was applied to center on specific ranges of wavenumbers where peaks of interest existed. Parameters such as laser power, acquisition time, and number of accumulations were adjusted to increase signal to noise ratio.

Surfaced Enhanced Raman Spectroscopy (SERS) was also performed to enhance spectra signal. For an extraction-less, directly-on-the-sample analysis, 0.5 μL of silver nanoparticles (AgNPs) produced using the procedure described by Lee and Miesel (1982) was applied on an ultramicroscopic sample *(7)*. The sample was then analyzed using the methodology described above for μRS.

3 Preliminary Results and Discussion

3.1 Pigment powder samples (raw pigments)

Red powder (Figure 18), from pigment ingots (Sample P1) and from pigment-containing shells (P2 and P3), was analyzed using PLM, pXRF (Figure 19), and XRD. PLM results of Samples P1 and P2 revealed the presence of specular hematite as indicated by the occurrence of reddish-brown granular particles identified as hematite associated with tabular flakes with shiny luster and quartz particles. XRD analysis confirmed the presence of hematite and quartz and has also suggested the presence of a calcium-based clay material. The results were further supported by XRF spectroscopy, determining the presence of Fe as the major element and Si and Ca as minor elements. Traces of Ti were also identified that might suggest the presence of a titaniferous mineral associated with hematite. Sample P2 also contained traces of another pigment (most likely an accidental contaminant due to depositional processes) with angular habit, intense red body color, and high relief. This red powder was identified as cinnabar, a mercury (II) sulfide compound (α-HgS). Its presence was further validated by XRF with the identification of Hg and S. Sample P3 was identified as pure cinnabar.

The specular hematite ingots (15 of them) found at this archaeological site are the first of this quantity and form to be recorded in the Maya region. The pigment is not indigenous to the area, which confirms that these ingots must have been imported from other parts of the Maya area such as central Mexico *(8)*. The scarcity of the pigment ingots is most likely due to their status as valued trade objects. Similarly, cinnabar is a very important and highly priced pigment that has been associated with burials of important Maya rulers and funerary rituals of venerated ancestors *(9-12)*.

3.2 Samples with evident red painted surface

In addition to raw pigment samples, the red color was also evident in painted surfaces of Samples 03, 04, and 05 (Figures 10, 11, and 12, respectively). Samples 03 and 05, described as clay that may have been used to wrap the body of the king, look very similar and were found near the same location in the tomb. Sample 04 (possibly a piece of painted stucco) is pigmented with a lighter red color. UV/Vis/NIR reflectance spectroscopy on all three samples revealed absorptions in the visible range indicative of electronic processes of Fe^{3+}, attributed to the presence of hematite. The typical characteristic absorptions in the visible and near infrared region seen for hematite occur between 521-565 nm and 848-906 nm. UV absorption results from ionic charge transfers (Fe^{3+}-O and Fe^{2+}-Fe^{3+}), which is the reason behind the red color of hematite *(13)*. XRF analysis confirmed the presence of Fe with higher concentrations in Samples 03 and 05. The red pigment in Samples 03 and 05 also appears brighter than the red found in Sample 04. This could be related to the occurrence of cinnabar, since Hg and S were also detected in Samples 03 and 05 using XRF and EDS. UV/Vis/NIR reflectance spectra of these strongly red-tinted layers clearly displayed the characteristic band-gap of S centered at ~610nm, confirming the presence of cinnabar.

3.2.1 Alteration of cinnabar-containing layer

Close examination of Sample 03 demonstrated evidence of degradation with the formation of black spots. These discolored areas in the red cinnabar-rich layer are rounded in shape with ~50 to 150 μm diameter (Figure 20). Under secondary electron (SE) imaging they appear granular, filled with conglomerate microbiological colonies (Figure 21), which are most likely contributing to the formation of the black staining.

Qualitative EDS spectra on the surface of the black spots showed significant levels of C, O, and Ca and depletion of S and Hg. BSE images of a polished cross-section of this area (Figure

22) indicated a pit crater in the sample (down to the clay body) with depth of approximately 50 μm and the deposition of microorganisms close to the walls of the crater. EDS spot analysis on the polished sample (Figures 22-23) confirmed the high levels of C, O, and Ca in the black regions and mainly Al and Si in the clay matrix. While the C and O could be easily attributed to the presence of organic matter and the Al and Si to the clay body, the occurrence of Ca is much less clear. It could potentially be a byproduct of microbiological metabolism in the form of calcium oxalate.

While these are only speculations, we suggest two possible pathways for the formation of the black stains: 1) the presence of microorganisms (bacteria, fungi, or algae, including cyanobacteria) that can cause the breakdown of the sulfide mineral leading to the biotransformation *(12)* or bioleaching *(14-16)* of Hg and 2) the presence of detoxification bacteria that can remove Hg by reduction of Hg^{2+} to Hg^{0} and final volatilization of Hg^{0} *(17-19)*. As the dark areas do not contain much of the original Hg and S, the staining may be of organic origin formed by microorganisms *(20,21)*.

3.3 Organic samples

Sample 02 (Figure 9) was described by the archaeologists as possibly bone mixed or coated with another material; however, photographs taken with the digital microscope suggest this sample may actually be a fragment of gourd, which was commonly used to make vessels. The cross-section of this sample looked morphologically similar to wood, with alternating dense and porous areas. The UV/Vis/NIR reflectance spectrum (Figure 24) shows absorptions at 1680, 1730, and 1760 nm corresponding to overtones (higher harmonics) of molecular fundamental vibrations of cellulose-based material, strengthening the hypothesis that this material may be gourd “wood”. However, further investigation is necessary to precisely match the organic signature of this material. The second derivative shows the minima and maxima of

the original absorption spectrum and enhances minute differences in the spectra by reducing the drift and noise of the baseline, which are caused by offsets in the direct current produced by the photodiode in the spectrometer as it converts transmitted or reflected light waves into current *(22,23)*. XRF analysis revealed the presence of some inorganic elements, such as Fe, Ca, P, and Si. Phosphorous is likely present on the sample from the decomposition of the human remains, while Fe, Ca, and Si may be present as a result of the burial soil that has cemented the fibrous material.

3.4 Sample with a lattice-shaped structure

Sample 06 (Figure 13), a dark brown porous sample, was recorded during excavation as a clay-based material. UV/Vis/NIR reflectance spectroscopy suggested the presence of clays and traces of organic materials. XRF analysis further indicated the presence of Hg.

SEM using SE imaging of a small piece separated from Sample 06 indicated a lattice-shaped (spongy looking) structure with needle-like crystals and spherical particles (50-80 μm in diameter) (Figure 25A-B). EDS analysis of the backbone spongy structure revealed the presence of Si and Al and traces of P, Ca, and Mg, while the spherical particles showed higher concentrations of P and Ca (Figure 25C) compared to the backbone structure.

The analysis of a polished cross-section indicated the presence of particles (assumed to correspond to the microspheres mentioned above) made of a system of concentric lamellae grouped together in circular arrangements (Figure 26). Elemental analysis and mapping of these circular features using EDS showed the characteristic X-ray emissions of Ca and P, suggesting the presence of a calcium phosphate phase (Figure 27). The results so far are preliminary and further analysis of this sample is required to provide more understanding about its precise identity and relationship to its archaeological context.

3.5 Green painted stucco fragment

Sample 09 (Figure 15) is a relatively thin sample with a green paint layer applied over a whitish layer (substrate). Brown residues beneath the white layer may indicate the presence of a wooden structure that has been lost, though further investigation is required for accurate attribution. It is believed to have decorated the bier on which the king was placed for burial. The sample was first analyzed non-invasively using hand-held XRF and UV/Vis/NIR reflectance spectroscopy from both sides. XRF results of the top layer (green) indicated the presence of Cu and, to a lesser extent, Ca and P. UV/Vis/NIR reflectance spectra (Figure 28) comparing [1] standard malachite ($CuCO_3(OH)_2$) to [2] the green layer in Sample 09 showed absorptions at ~800 nm and 1300 nm corresponding to electronic transitions of Cu ions and between 2200 and 2400 nm indicative of the CO_3 and OH groups, respectively, characteristic of malachite. The presence of malachite was also confirmed using X-ray diffraction (Figure 29). An absorption at ~1920 nm in the UV/Vis/NIR spectrum is likely due to the presence of water within the sample. XRF results of the white substrate showed Ca and P with less evident traces of Cu. UV/Vis/NIR reflectance spectroscopy has yielded interesting results in the organic region with small absorptions corresponding to the first overtones of CH stretching, suggesting the presence of organic matter in the white substrate.

The examination of a polished section of this sample (Figure 30A) using VPSEM clearly revealed the two distinct layers: a green layer (top) appearing brighter under BSE detection (Figure 30B-C) and a Ca and P-rich layer (substrate) consisting of angular aggregates in a microcrystalline matrix (Figure 31D). Examination of this sample using high resolution digital microscopy (Figure 30A) clearly revealed two distinct layers: a vivid green layer (top) of approximately 100 microns and a white layer (substrate) with angular aggregates in a microcrystalline matrix of approximately 0.7 mm. VPSEM-EDS of a cross section of Sample 09 showed – as expected – the characteristic x-rays for copper in the green paint layer (appearing

brighter under BSE detection) (Figure 30B-C) and calcium and phosphorous in the aggregates of the thin white substrate (Figure 30D). The shape and composition of these aggregates points towards the use of crushed bones in the plaster/stucco layer. Raman analysis on the same particle, confirmed the presence of bone with a Raman shift at 960 cm-1 indicative of phosphates and a shoulder at ~1077 cm^{-1} characteristic of carbonates (Figure 30E). The results obtained by these combined techniques suggest that the bier on which the king was resting, made most likely of wood that was perished by the burial environment, was decorated with a thin stucco/plaster layer made of crushed bones and painted with malachite (green copper pigment). While the origin of the bones (whether animal or human) has not yet been confirmed, the relation between these bone aggregates in the plaster and the human phalanges found inside ceremonial vessels (within whitish/grey dust) from the same tomb is currently investigated. DNA analysis will also be conducted to identify whether the bone fragments in the white stucco layer are either human or animal.

3.6 White Powder in Vessels

Outside of tomb 9, some of the lip-to-lip closed vessels contained whitish-grey powder resembling pulverized bone that covered an intermediate manual phalanx and a left mandibular central incisor (Figure 17). A sample of this powder was analyzed using XRF, resulting in high concentrations of Ca and O in ratios indicative of $CaCO_3$. However, few small bone fragments were found dispersed in the powder. SEM imaging of a bone fragment in low vacuum mode revealed typical bone-like morphology (Figure 31), and EDS mapping confirmed the presence of Ca, P, and O consistent with hydroxyapatite (Figure 32).

4 Conclusion

The scientific protocol behind this study, based on minimally invasive, non-destructive micro-analytical techniques, was important for the preliminary characterization of fragile archaeological samples. Though most of the work done so far has been primarily qualitative, these initial findings on the morphology, elemental composition, and molecular structure of the excavated samples provide invaluable information on the original materials.

New information on the materials used in funerary decoration and as burial offerings was brought to light, particularly in the use of bone being crushed to form ornamental stucco and the identification of cinnabar and exotic specular hematite unique in form and quantity. The use of cinnabar and specular hematite in *spondyllus* shells, suggest a direct association with elite Maya burials and funerary rituals *(2,5,8,24,25)*. The identification of bone in mortuary decoration is new to the literature. However findings such as child sacrifices, severed digits and blades to saw bone in burial 9 at El Zotz, support the hypothesis of the ritualistic use of bone meal for the decoration of this elite burial.

Further systematic analysis of all samples with microanalytical techniques will provide more detailed chemical characterization. Other specific points that will receive further detailed study include: the mechanisms and kinetics for cinnabar degradation in Sample 03, provenance investigations to reveal the origin of the specular hematite in Samples P1 and P2, further investigations on the Hg presence in Sample 06 and identification of the lattice-shaped structure and microspheres in the context of the burial and funerary paraphernalia, and DNA (ancient DNA) testing of the bone fragments found in Sample 09. Conclusive information regarding these specific points and an overall more comprehensive study of all samples will provide the necessary insight into the culture and practices of this ancient civilization.

5 Figures

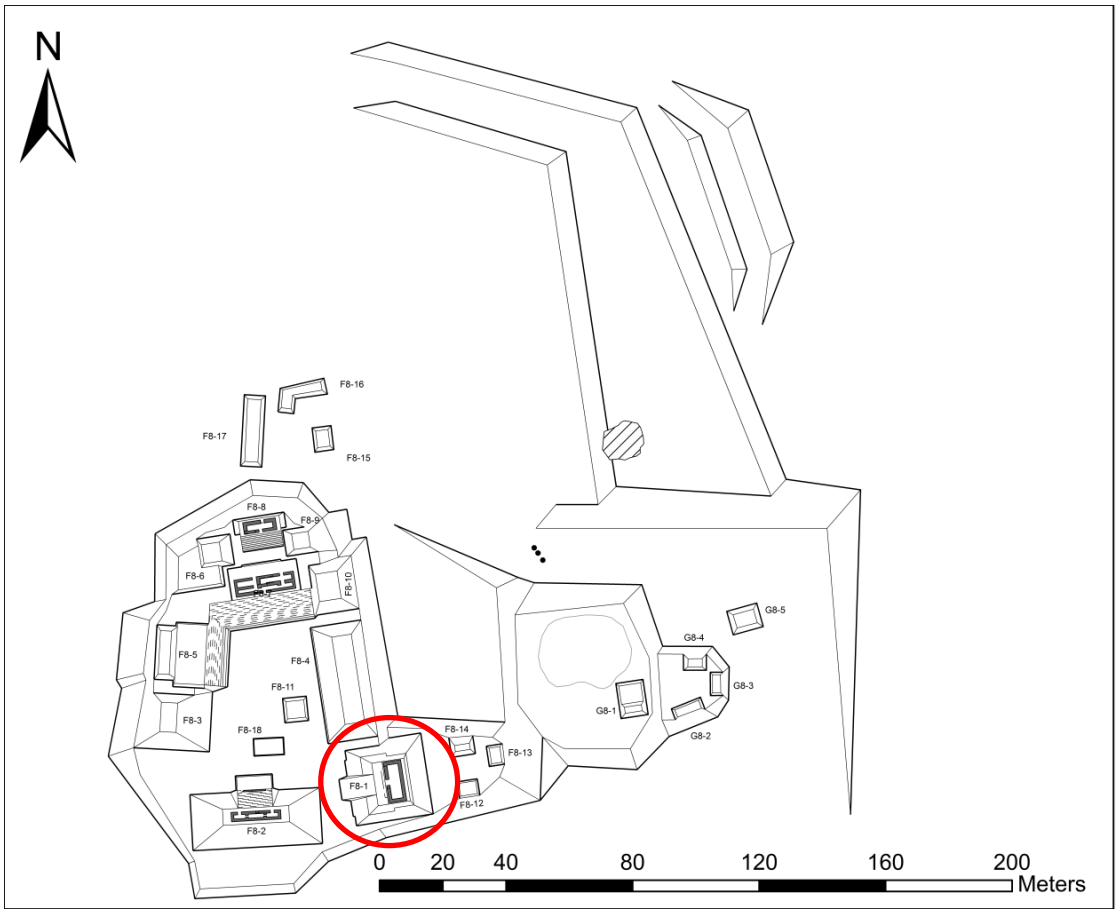

Figure 1. Map of the El Diablo complex of El Zotz, showing structure F8-1 where Burial 9 was found. (Drawing by Thomas Garrison)

Figure 2. Stucco mask decorating structure F8-1. (Courtesy of Arturo Godoy)

Figure 3. Detail of stucco mask on structure F8-1. (Courtesy of Arturo Godoy)

Figure 4. Discovery of Burial 9 found within structure F8-1, revealing a plethora of ornate funerary objects. (Courtesy of Arturo Godoy)

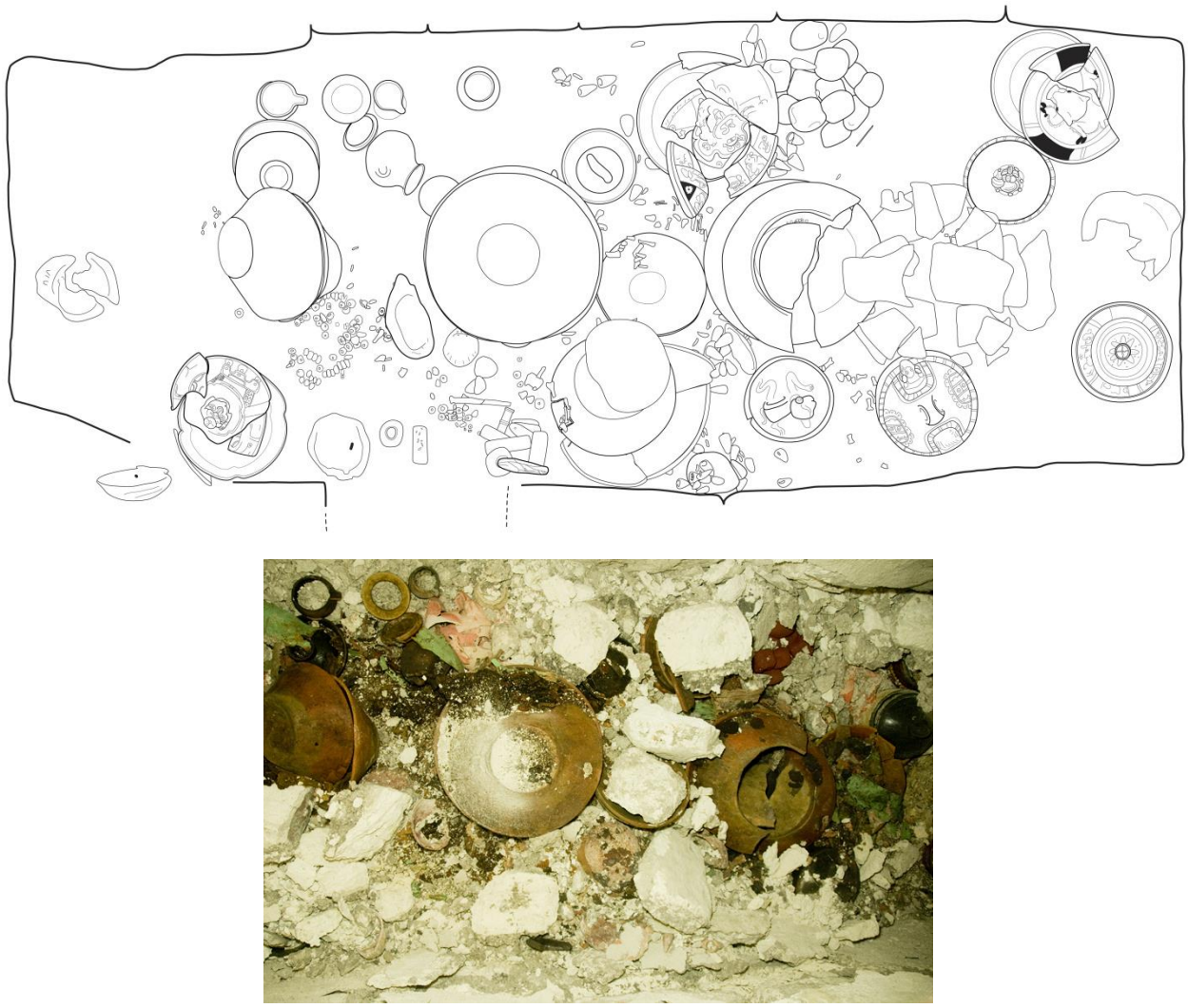

Figure 5. Archaeologist's drawing of artifacts found in burial 9, photographed below. (Drawing courtesy of Sarah Newman, Photo courtesy of Arturo Godoy)

Figure 6. Orange lip to lip vessels, some of which housed these human remains, cubes of hematite (iron oxide) trade pigment and painted stucco masks. (Courtesy of Sarah Newman)

Figure 7. Human remains found inside burial 9. (Courtesy of Andrew K. Scherer)

Figure 8. SAMPLE 01: ***Remains of some kind of basket; possibly cord.*** *Stereomicroscope observations: off-white/cream color with some brown areas; fragile, porous structure; orange-brown surfaces with white particles.*

Figure 9. SAMPLE 02: ***Possibly bone, seemingly or mixed with another material.***
Stereomicroscope observations: brown clay-like color and texture; porous; white particles sprinkled throughout the surface.

Figure 10. SAMPLE 03: ***Clay and pigment that may have been used to wrap the body.***
Stereomicroscope observations: top side – brown body with red color on surface; bottom side – brown with white particles; spongy and porous structure; clay/earth-like texture; with white fibers and iridescent spots.

Figure 11. SAMPLE 04: ***Clay and pigment/painted stucco that may have been below the body.***
Stereomicroscope observations: top side - pinkish color; bottom side – dark black/brown color with white particles; porous structure; web of white fiber on surface.

Figure 12. SAMPLE 05: ***Clay and pigment that may have been used to wrap the body.***
Stereomicroscope observations: dark brown areas with bright red/orange paint; clay-like material; grey web-like fibers on surface; areas of iridescent black spots; dispersed white particles.

Figure 13. SAMPLE 06: ***Clay matrix.***
Stereomicroscope observations: dark brown with web-like structure; whitish and yellow particles on the surface.

Figure 14. SAMPLES 07 & 08: ***Remains of some kind of cordage.***
Stereomicroscope observations: dark brown matrix with parallel striations; wood-like; possibly basket; contains white spherical particles and silver-like threads dispersed throughout.

Figure 15. SAMPLE 09: ***Green painted stucco fragments.***
Stereomicroscope observations: top side – green paint and brownish yellow debris on the top; dark green line across green surface with corresponding darker brown line on back side of fragment; bottom side – whitish layer; plaster-like.

Figure 16. SAMPLE 10: ***Some kind of grey material with impressions.***
Stereomicroscope observations: off-white surface with grainy areas of dark brown/black color; white particles dispersed throughout; pseudomorphic textile texture; powdery white particles on edges.

Figure 17. SAMPLE 11 (Archaeologist Accession Number EZ-19A-10-2): ***White powder from lip-to-lip cache vessel, covering an intermediate manual phalanx (adult) and a left mandibular central incisor (well-preserved).***
Stereomicroscope observations: white/grey condensed powder broken in fragments.

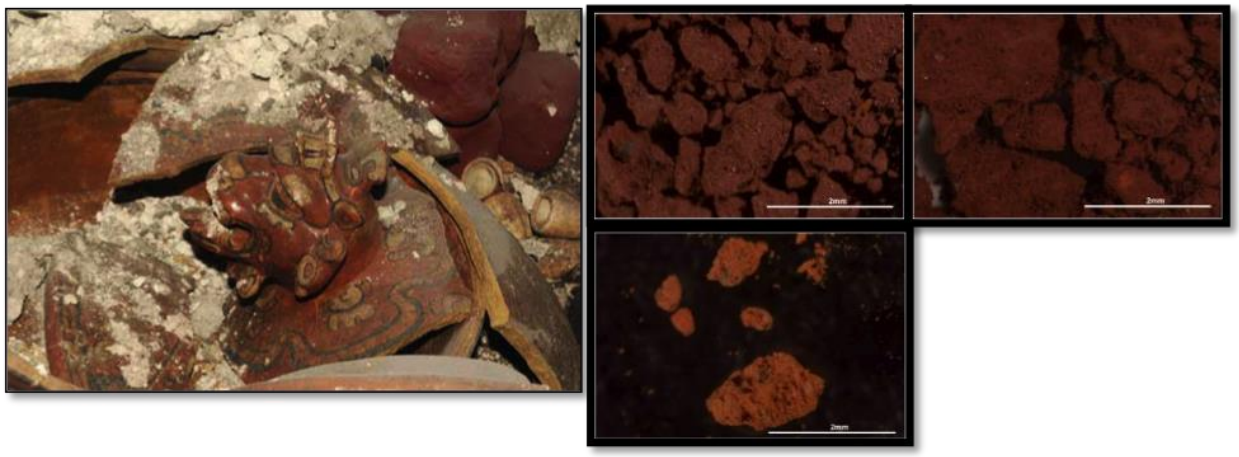

Figure 18.
(A) SAMPLE P1: ***Pigment from cubes.***
Polarized light microscope observations: largely containing brick red particles and tabular black translucent particles (perhaps specular hematite) and specks of white particles.
(B) SAMPLE P2: ***Pigment from spondylus shell.***
Polarized light microscope observations: brick red particles with a few distinctive orange particles and black translucent tabular particles (perhaps specular haematite) and a few white friable particles; few hard pebble-like particles are also present.
(C) SAMPLE P3: ***Unknown pigment associated with shell necklace.***
Polarized light microscope observations: mainly orange particles with yellowish/brownish impurities (possibly organic).

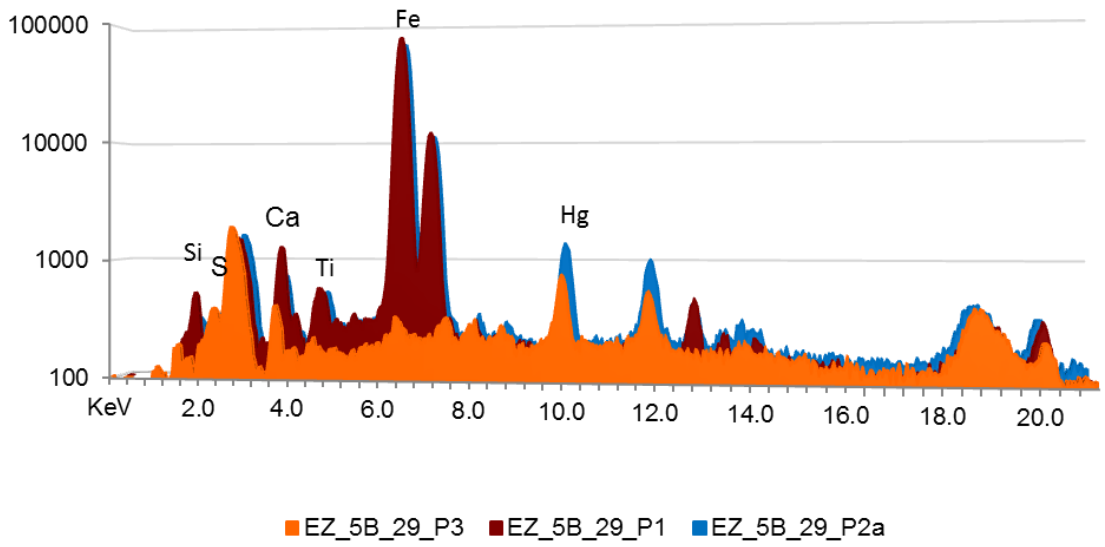

Figure 19. Portable XRF spectra (counts (log) vs. energy in keV) of pigments Samples P1 (light grey patterned spectrum), P2 (solid black spectrum), and P3 (solid grey spectrum). P1 and P2 are almost identical, showing high Fe content and minor Si and Ca. Characteristic X-ray lines for Hg and S in P2 and P3 spectra are attributed to the presence of cinnabar.

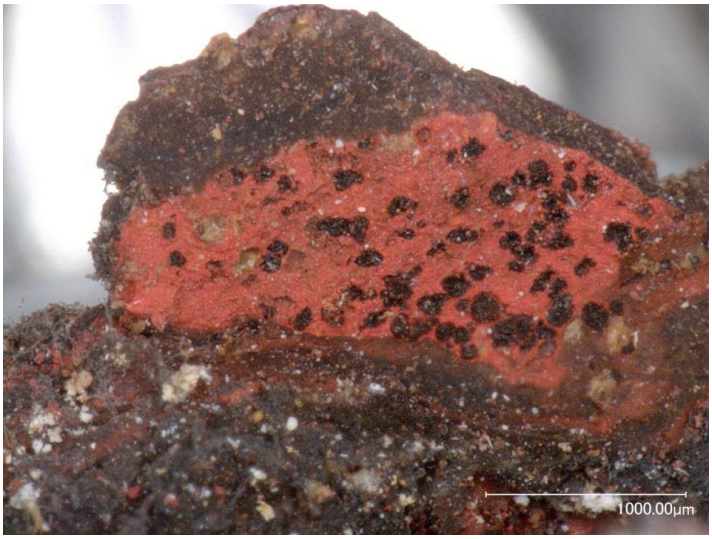

Figure 20. Digital micrograph of Sample 03 at 100x magnification, showing cinnabar alteration with black spots.

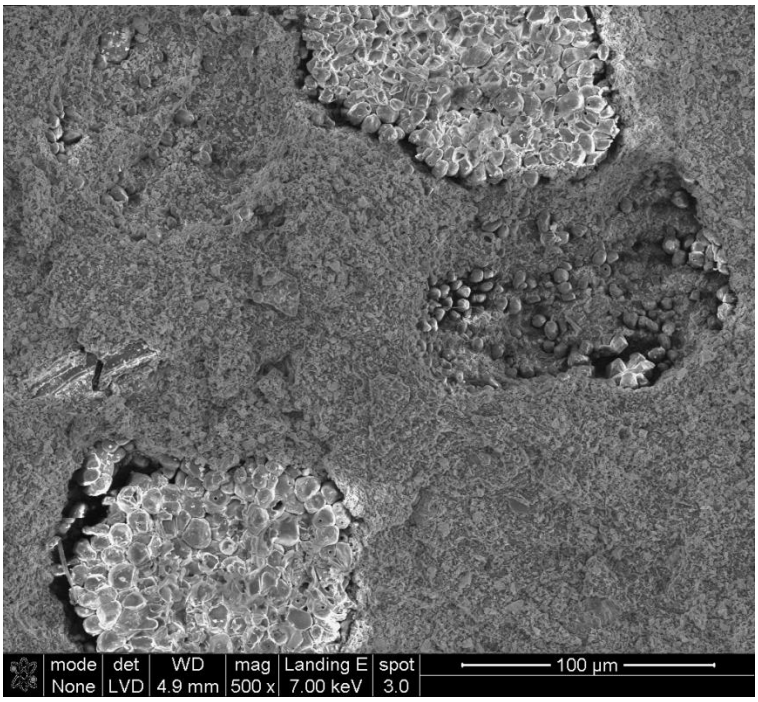

Figure 21. SE image of biological colonies found in black regions of cinnabar on Sample 03.

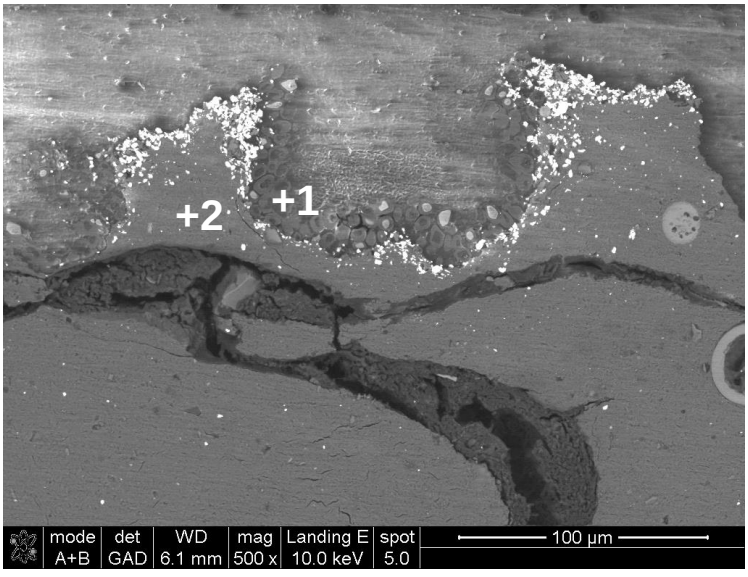

Figure 22. BSE image of a cross sectional view of Sample 03, showing remnants of cinnabar (bright particles) near the pit crater-like formation with microorganisms at the bottom and side walls.

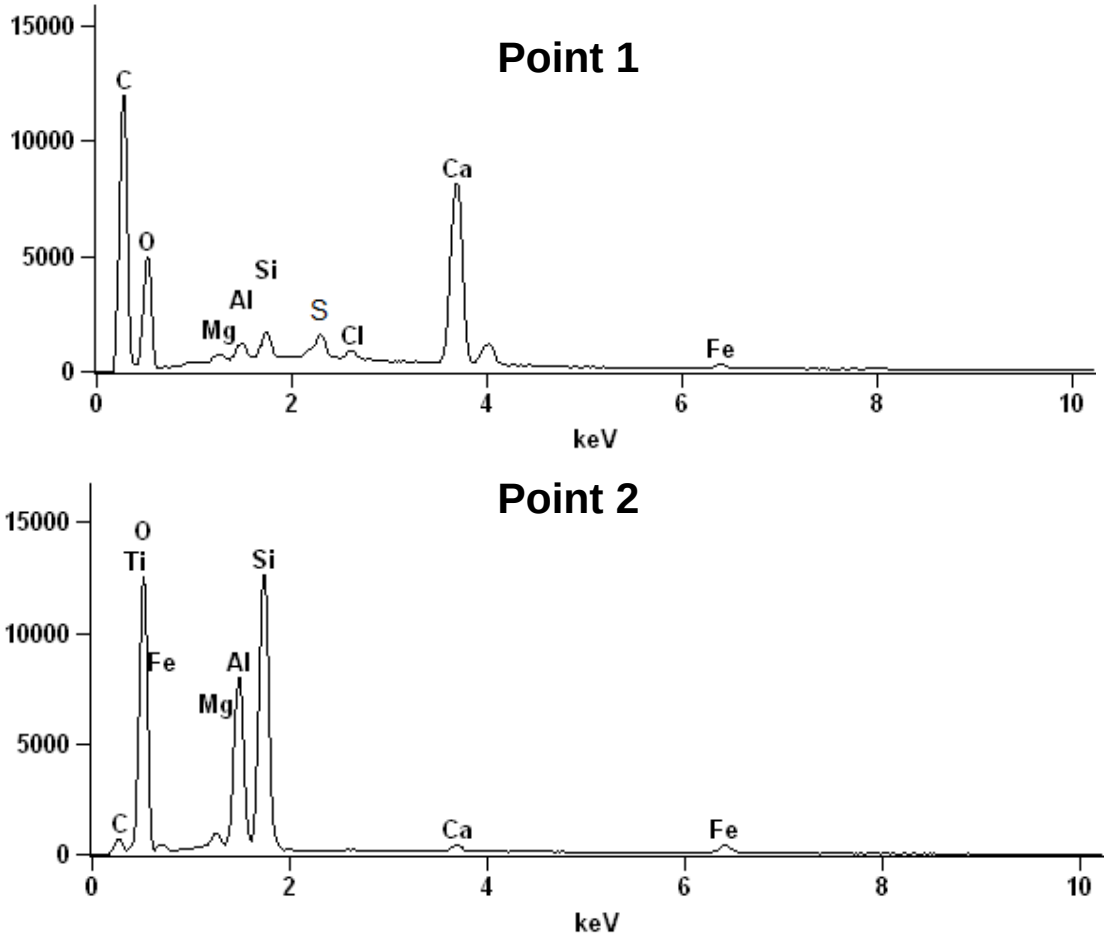

Figure 23. (Top) EDS spectrum of biological black regions in Sample 03, showing intense characteristic X-ray emissions of C, O, and Ca. (Bottom) EDS spectrum of the clay matrix beneath the cinnabar layer with major elements, Al and Si.

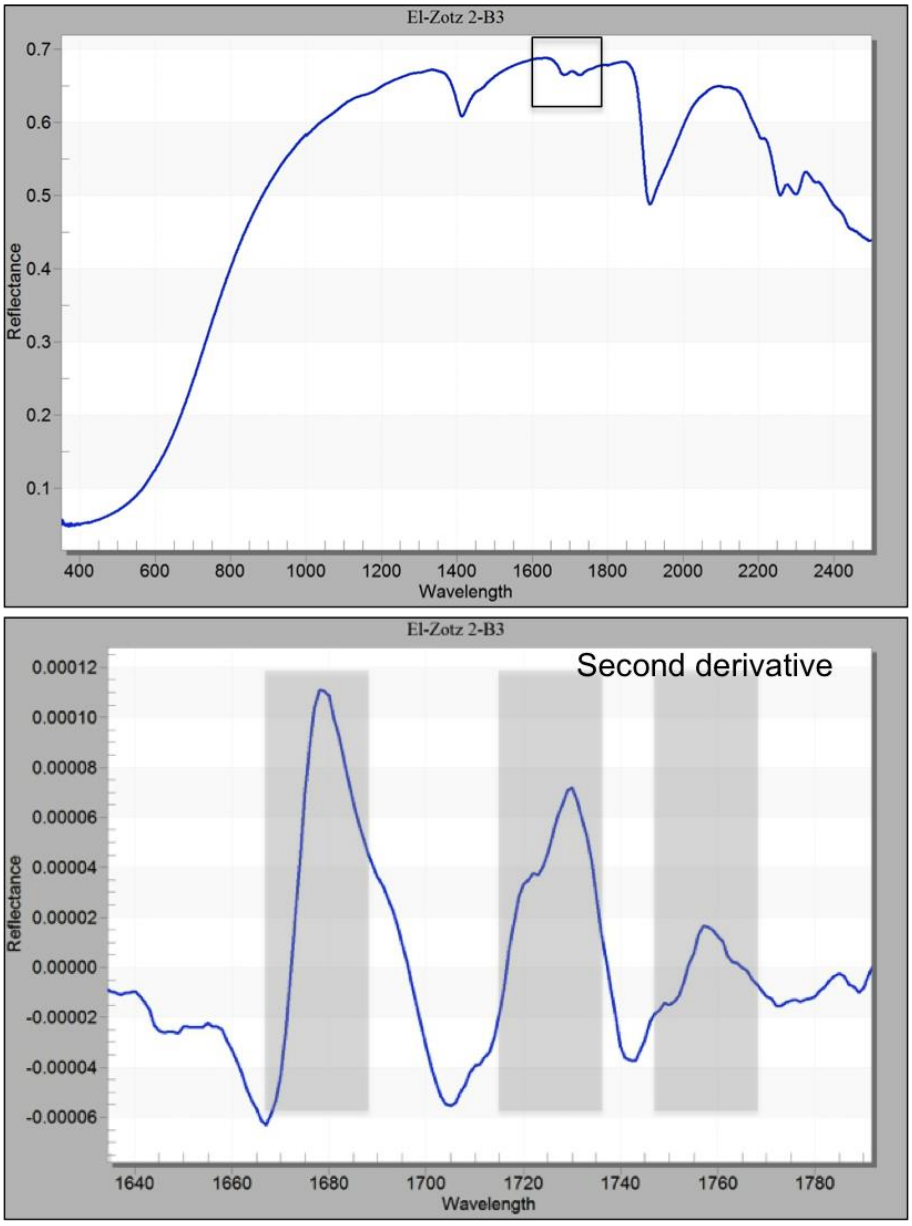

Figure 24. UV/Vis/NIR reflectance spectrum of Sample 06 (top), with the second derivative of boxed region (bottom). Positive peaks of the second derivative correspond with absorptions in the original spectrum and show the first overtone of C-H stretching vibration (2v C-H) of cellulose-based material at 1680, 1730, and 1760 cm^{-1}.

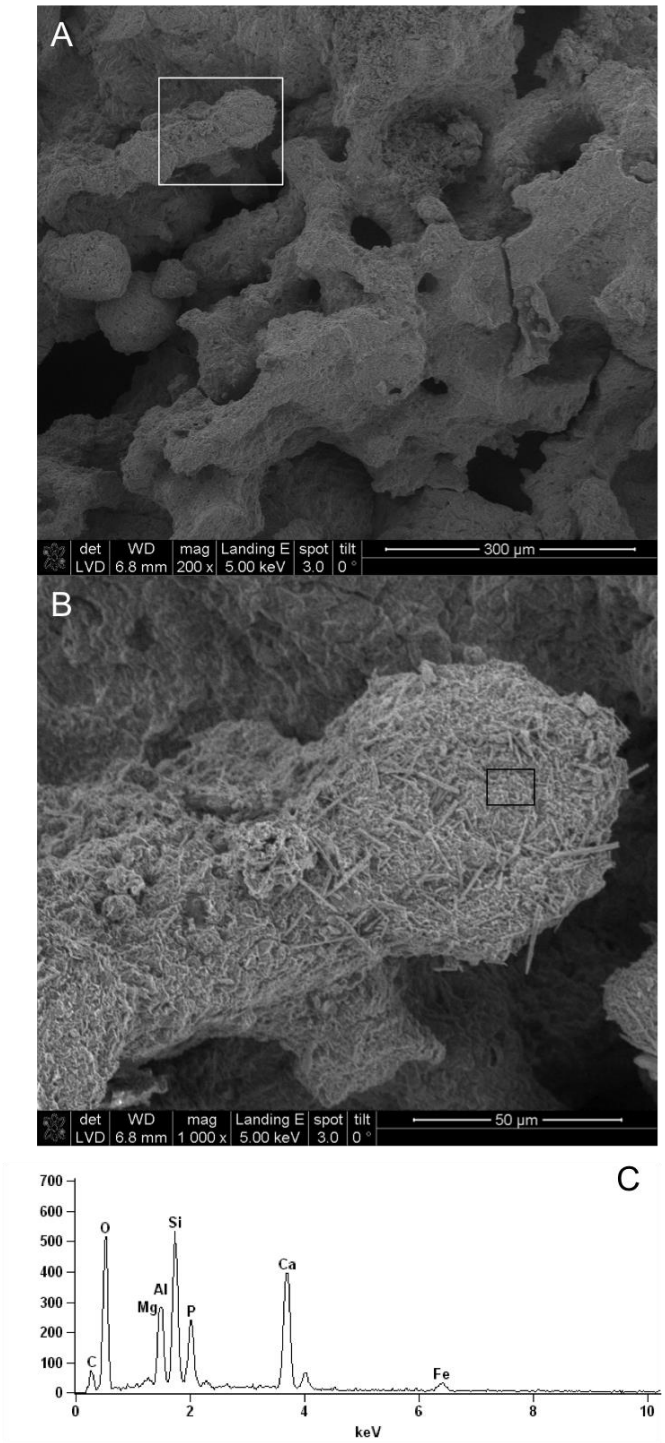

Figure 25. SE micrograph (Image A) of a detail of Sample 06 showing the lattice-shaped (spongy) structure. The white square indicates the area magnified in micrograph B showing the needle-like crystals and one of the spherical-shaped particles. Image C shows a spectrum of the elemental composition of the spherical particle within the area marked with a black square, showing Ca, Si, O, P, and Al as the major elements with C, Mg, and Fe as minor elements.

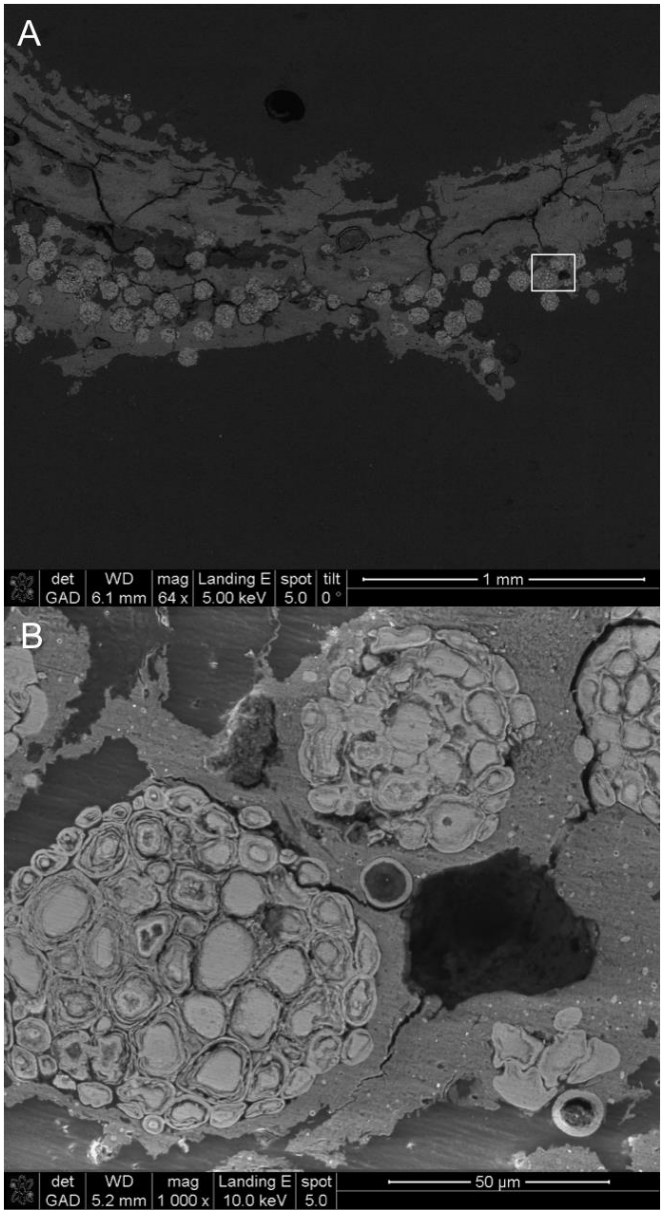

Figure 26. Image A shows the BSE micrograph of a cross-sectional view of a small piece of Sample 06. Image B is a BSE detail view of the white square in Image A, with sphere-shaped clusters and quill-like structures.

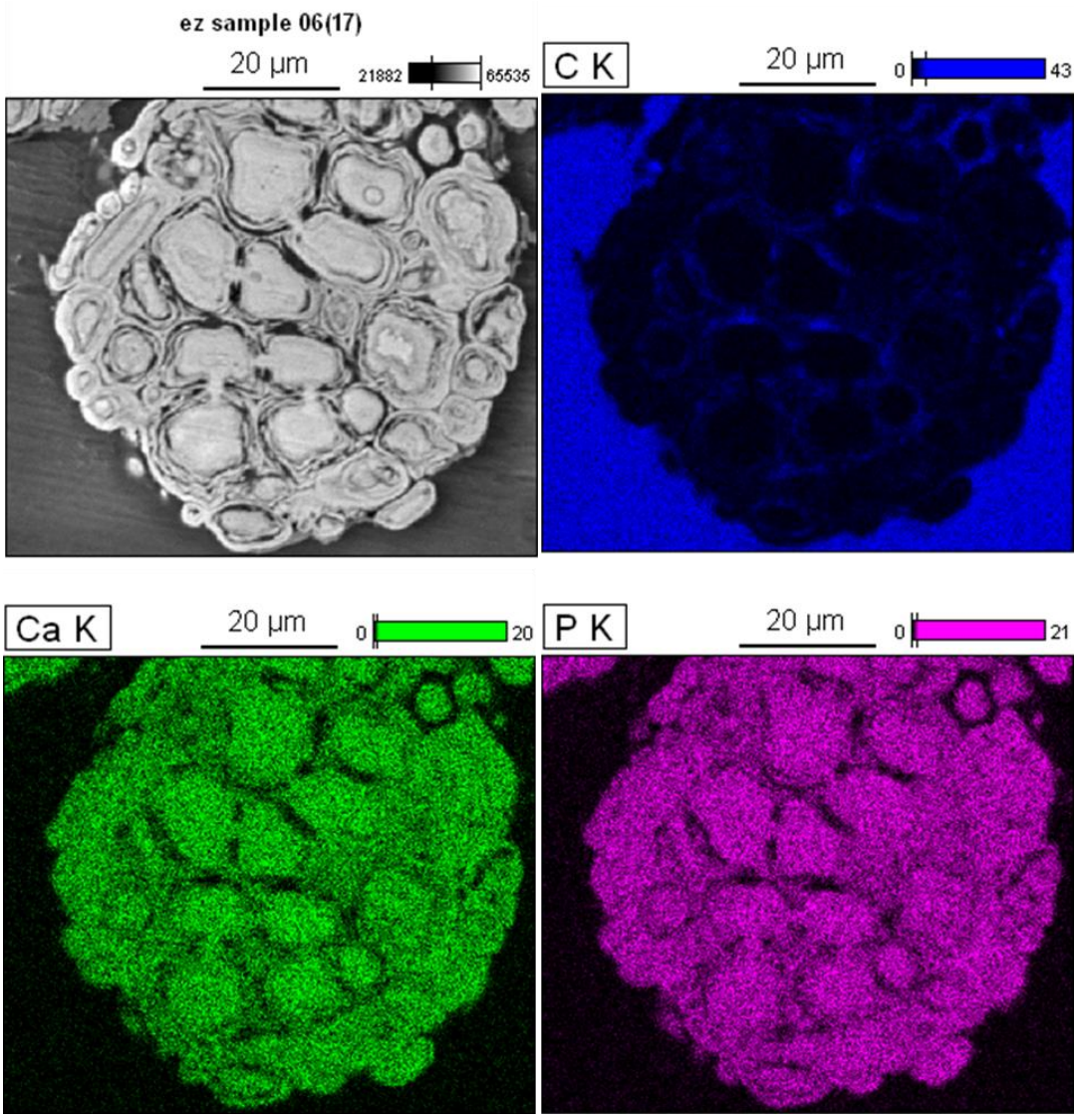

Figure 27. BSE micrograph (top left) and EDS elemental maps on a cross-sectional view of one of the spherical particles, showing the spatial distribution of the predominant elements detected: C, Ca and P. Ca and P are the major elements found in these spherical structures (pointing towards a calcium phosphate mineral) while C corresponds to the voids filled with resin.

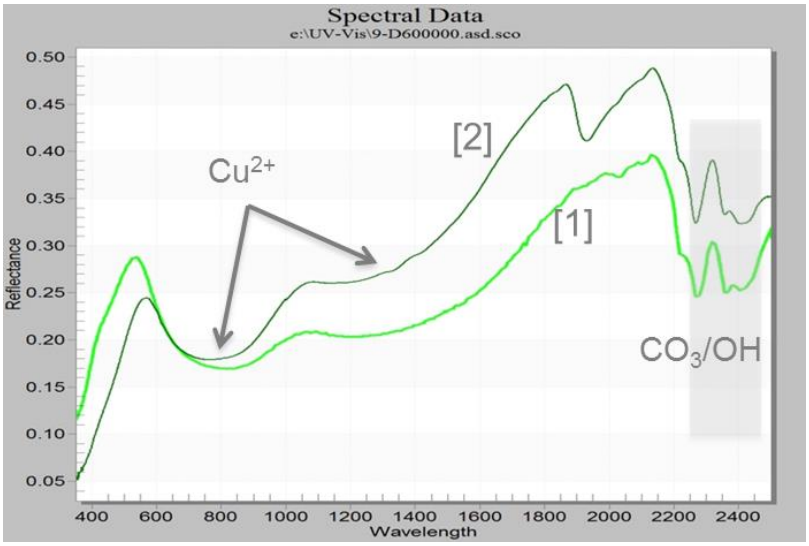

Figure 28. UV/Vis/NIR reflectance spectra comparing [1] standard malachite to [2] the green pigment in Sample 09.

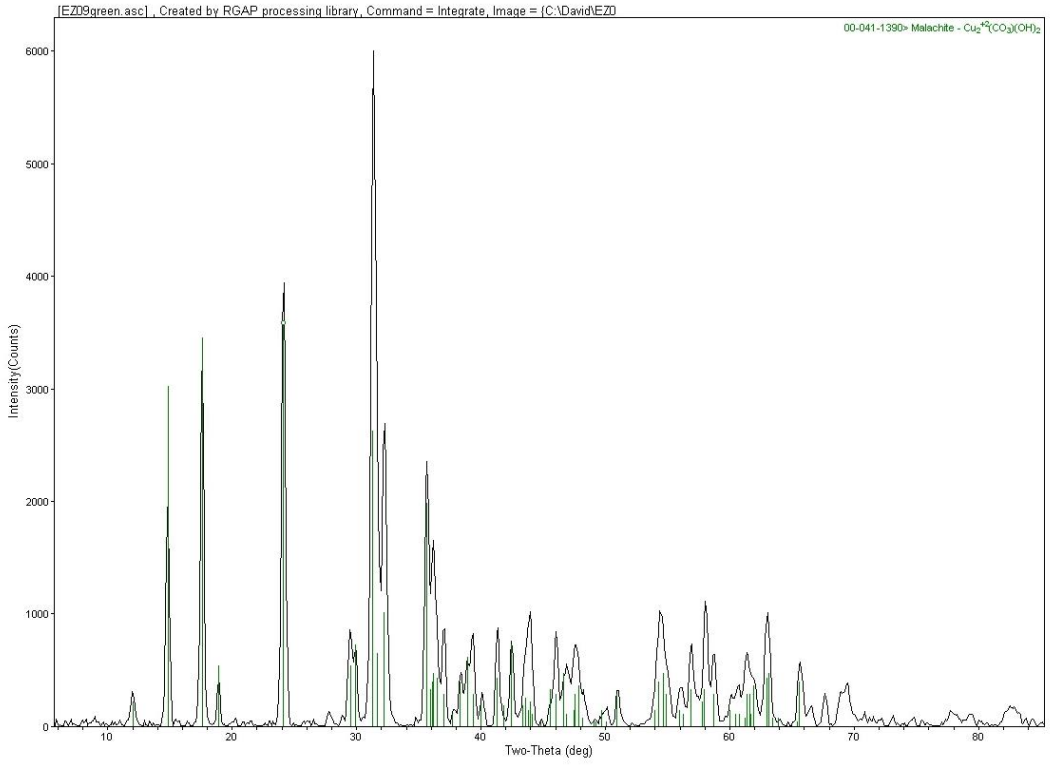

Figure 29. XRF spectrum confirming malachite as the green painted layer.

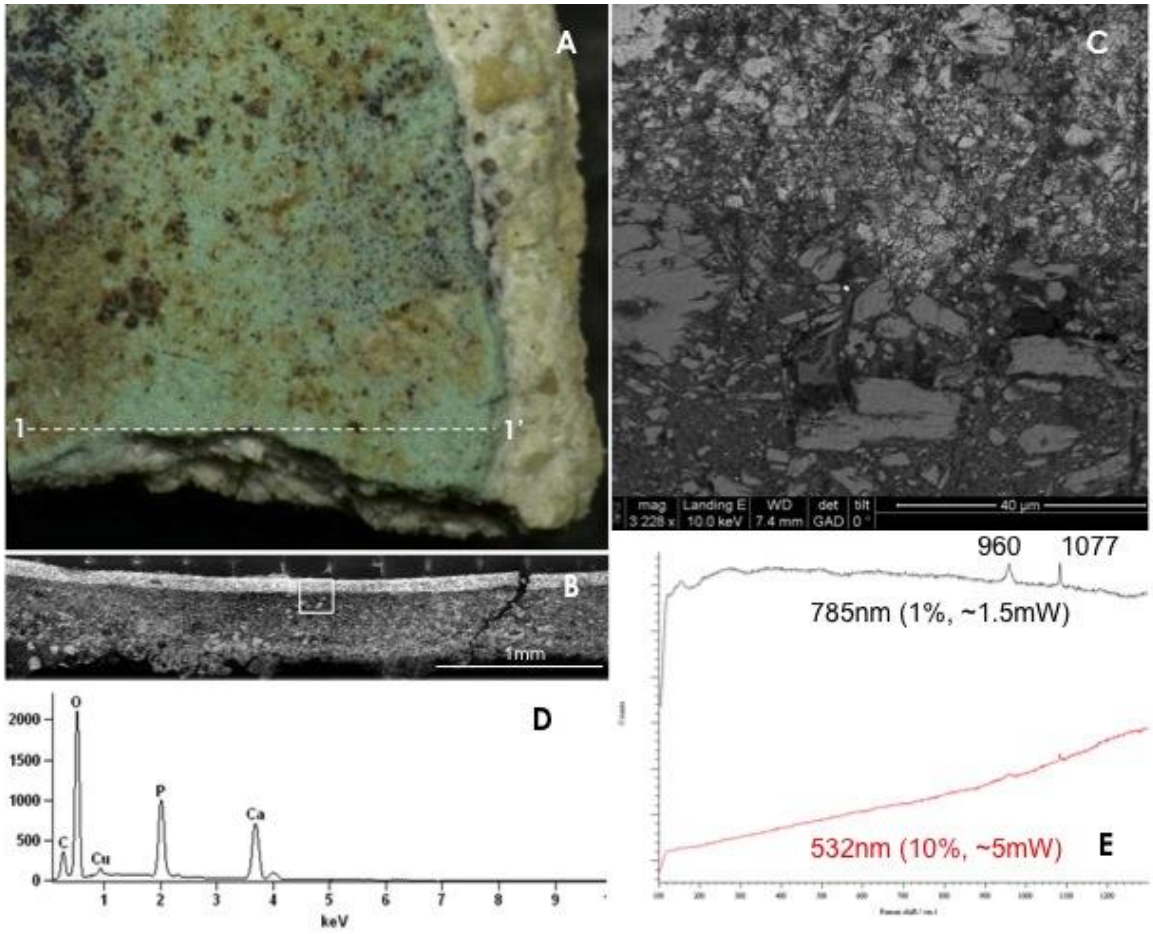

Figure 30. Photomicrograph of sample 09 (A) showing the green malachite layer and the white stucco layer. Dotted line 1-1' indicates the area sectioned for the preparation of a cross section (B). BSE micrograph (C) of the area marked with a white square in image B illustrating the interface between the green layer and the stucco layer. EDS spectrum of the aggregate in the stucco layer showing the characteristic x-rays for phosphorus (P) and calcium (Ca) (D) and Raman spectra of the same aggregates using 785 and 532 nm excitation showing the presence of hydroxyapatite and carbonate minerals (E).
Peaks are labeled by wavenumbers.

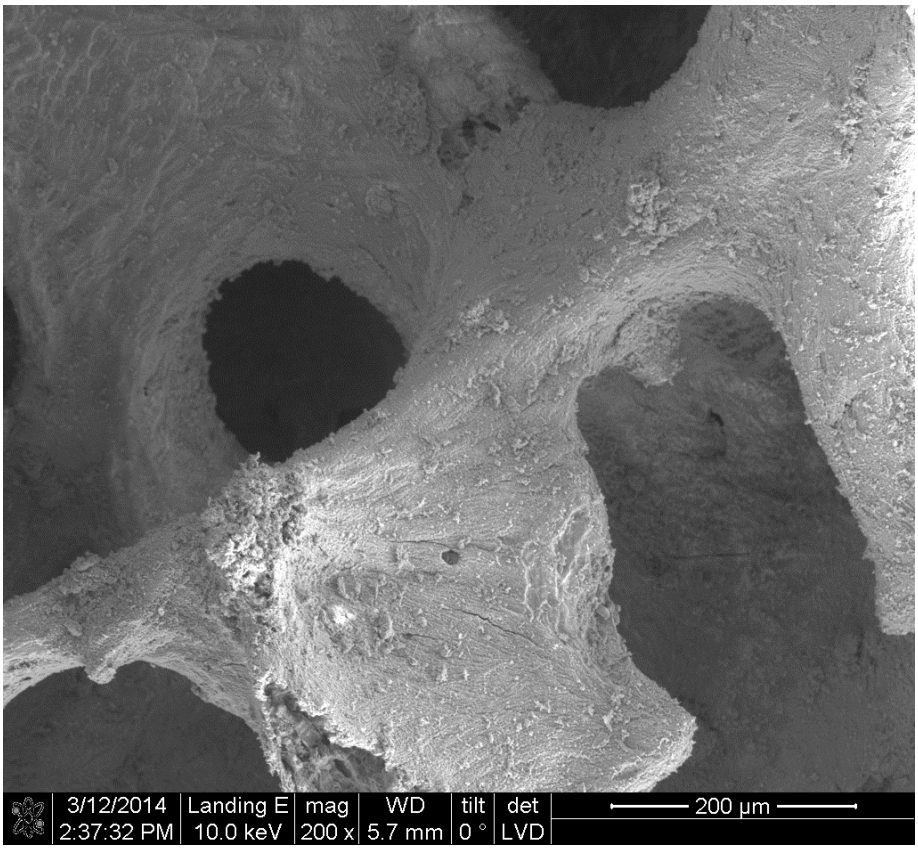

Figure 31. Bone fragment from EZ-19A-10-2 sample of white powder from lip-to-lip cache vessel under variable pressure SEM. Powder was covering an intermediate manual phalanx (adult) and a well-preserved left mandibular central incisor.

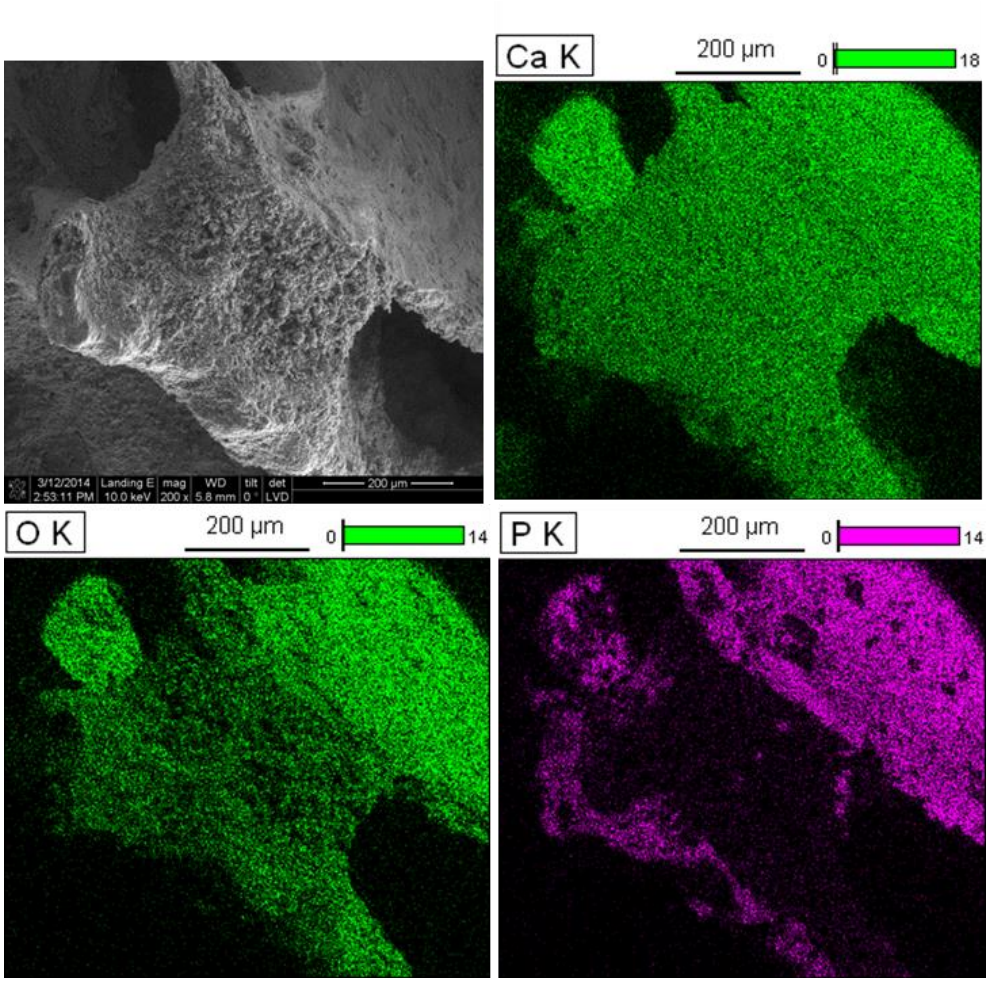

Figure 32. EDS maps of bone fragment, confirming hydroxyapatite elemental composition (Ca, P, and O).

6 References

1. Houston, S.; Nelson, Z.; Escobedo, H.; Meléndez, J.C.; Arroyave, A.L.; Quiroa, F.; Cambranes, R. *Levantamiento preliminar y actividades de registro en El Zotz, Biotopo San Miguel La Palotada, Petén*, 2006, Departamento de Monumentos Prehispánicos y Coloniales, Dirección General del Patrimonio Cultural y Natural de Guatemala.

2. Román-Ramírez, E.R. *Living the sacred landscape: the process of abandonment of the Early Classic Maya group of El Diablo at El Zotz, Petén, Guatemala*, in *Latin American Studies,* 2011, University of Texas: Austin.

3. Houston, S. *Segunda Temporada de Campo en El Zotz: Introducción. In: Proyecto Arqueológico El Zotz, Informe No. 2, Temporada 2007.* , S. Houston, H.L. Escobedo, and J.C. Meléndez, Editors. 2007, Dirección General del Patrimonio Cultural y Natural de Guatemala.

4. Houston, S.; Escoberdo, H.L.; Meléndez, J.C. *Proyecto Arqueológico El Zotz: Informe No.2, Temporada 2007.* , S. Houston, et al., Editors. 2007, Dirección General del Patrimonio Cultural y Natural de Guatemala.

5. Houston, S., *Final Performance Report: In the Shadow of a Giant: Archaeology of El Zotz, Guatemala*, 2011, National Endowment for the Humanities.

6. Plesters, J. *Stud. Conserv.* **1956**, *2(3)*, 110-157.

7. P. C. Lee and D. Meisel, *J. Phys. Chem.*, 1982, **86**, 3391.

8. Moholy-Nagy, H. *J. Field Archaeol.* **1997**, *24*, 293-313.

9. Chelazzi, D.; Poggi, G.; Jaidar, Y.; Toccafondi, N.; Giorgi, R.; Baglioni, P. *J. Colloid Interface Sci.* **2013**, *392*, 42-29.

10. Kelly, D.; Budd, K.; Lefebvre, D.D. *Appl. Environ. Microbiol.* **2006**, *72*, 361-367.

11. Kapridaki, C.; Maravelaki-Kalaitzaki, P. *Prog. Org. Coat.* **2013**, *76*, 400-410.

12. Lefebvre, D.D.; Kelly, D.; Budd, K. *App. Environ. Microbiology*. **2007**, *73*, 243-249.

13. Popelka-Filcoff, R. S.; Mauger, A.; Lenehan, C. E.; Walshe, K.; Pring, A. (2014). *Analytical Methods*. **2014**, *6*(5), 1309.

14. Bosecker, K. *FEMS Microbiol. Rev.* **1997**, *20(3-4)*, 591-604.

15. Hansford, G. S.; Vargas, T. *Hydrometallurgy* **2001**, *59(2)*, 135-145.

16. Suzuki, I. *Biotechnol. Adv.* **2001**, *19(2)*, 119-132.

17. Wagner-Döbler, I. *Appl. Microbiol. Biotechnol.* **2003**, *62(2-3)*, 124-133.

18. Mathema, V. B.; Thakuri, B. C.; Sillanpää, M. *Arch. Microbiol.* **2011**, *193(12)*, 837-844.

19. Nascimento, A. M.; Chartone-Souza, E. *GMR, Genet. Mol. Res.* **2003**, *2(1)*, 92-101.

20. Martin-Sanchez, P. M.; Sanchez-Cortes, S.; Lopez-Tobar, E.; Jurado, V.; Bastian, F.; Alabouvette, C.; Saiz-Jimenez, C. *J. Raman Spectrosc.* **2012**, *43(3)*, 464-467.

21. Vasanthakumar, A.; DeAraujo, A.; Mazurek, J.; Schilling, M.; Mitchell, R. *Int. Biodeterior. Biodegrad.* **2013**, *79*, 56-63.

22. Luthria, D.; Mukhopadhyay, S.; Lin, L.; Harnly, J. *Appl Spectrosc.* **2011**, 65(3), 250–259.

23. Chen, Q.; Zhao, J.; Zhang, H.; Wang, X. (2006). *Analytica chimica acta*, **2006,** 572(1), 77–84.

24. Houston, S.; Román, E.; Garrison, T.G.; Garrido, J.L.; Carter, N.; Doyle, J.; Menéndez, E.D.; Newman, S.; Kingsley, M. *En la vista de Pa´Chan: procesos Dinámicos en El Zotz, Petén y sus Cercanías*, 2010.

25. Houston, S.; Román, E.; Garrison, T.G.; Garrido, J.L.; *Introducción*. *In Proyecto Arqueológico El Zotz, Informe 5 Temporada de Campo 2009*, G. Pérez, E. Román, and S. Houston, Editors. 2009, Instituto de Antropología e Historia de Guatemala.